Precise targeting of *POLR2A* as a therapeutic strategy for human triple negative breast cancer

Jiangsheng Xu, Yunhua Liu, Yujing Li, Hai Wang, Samantha Stewart, Kevin van der Jeught, Pranay Agarwal, Yuntian Zhang, Sheng Liu, Gang Zhao, Jun Wan, Xiongbin Lu, Xiaoming He

Supplementary Figures

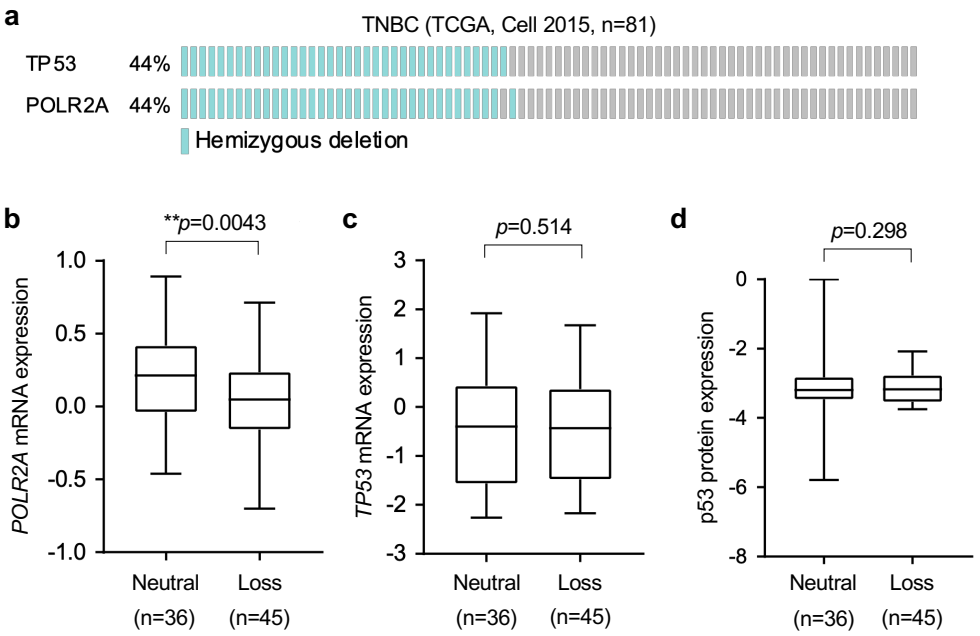

Supplementary Fig. 1. Colateral deletion of *POLR2A* with *TP53* in triple negative breast cancers. **a**, Concomitant deletion of *POLR2A* in human TNBC samples (TCGA, Origin: Cell 2015) containing hemizygous loss of *TP53* (n=X biologically independent samples). **b-d**, The correlation of POLR2A mRNA (**b**), p53 mRNA (**c**), or protein (**d**) expression with copy number variation in TNBC samples. TCGA: The Caner Genome Atlas (http://atlasgeneticsoncology.org/tcga_projects.html), and TNBC: triple negative breast cancer. The statistical significance was assessed by Student's *t*-test (unpaired, two-tailed). The Box-Whisker plots present a five-number summary: minima, lower quartile, centre, upper quartile, and maxima. **, $p < 0.01$.

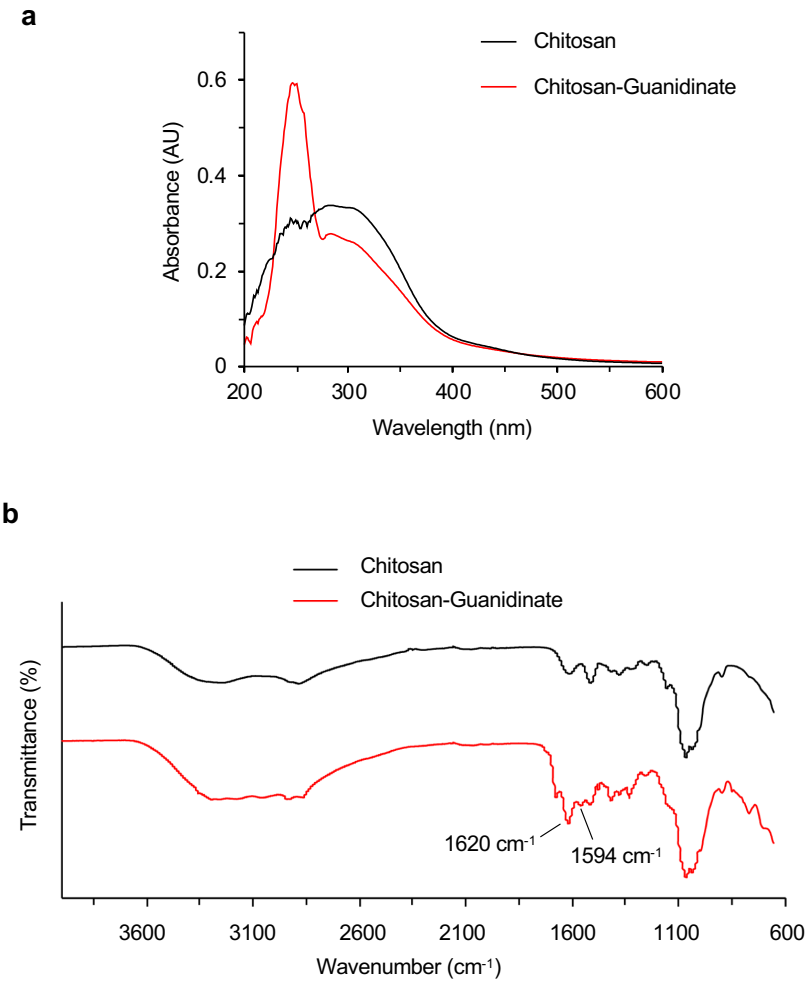

Supplementary Fig. 2. Characterization of the modification of chitosan with guanidine. a, UV-vis absorbance of chitosan before (black) and after (red) modification with guanidine. The specific absorption peak at 245 nm of guanidine in chitosan-guanidinate indicates the successful modification of guanidine onto chitosan. **b,** FTIR spectra of chitosan and chitosan-guanidinate showing the absorption of guanidine group at 1594 cm^{-1} and 1620 cm^{-1}. UV-vis: ultraviolet-visible light, and FTIR: Fourier transform infrared spectroscopy. The experiments were repeated three times independently.

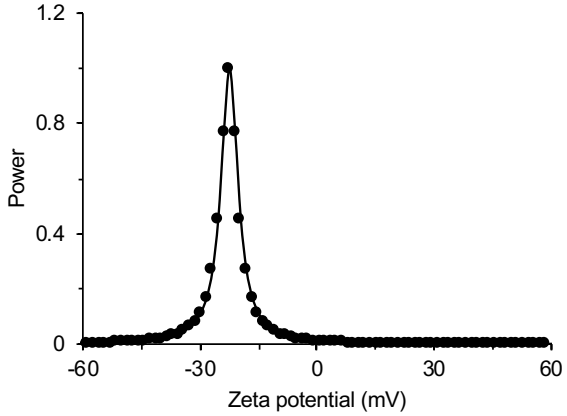

Supplementary Fig. 3. Zeta potential of siPol2-laden nanoparticle. Zeta potential (-22.4 ± 2.1 mV, mean ± s.d.) of the siPol2-laden nanoparticles (siPol2@NPs) in deionized water (n=3 independent experiments).

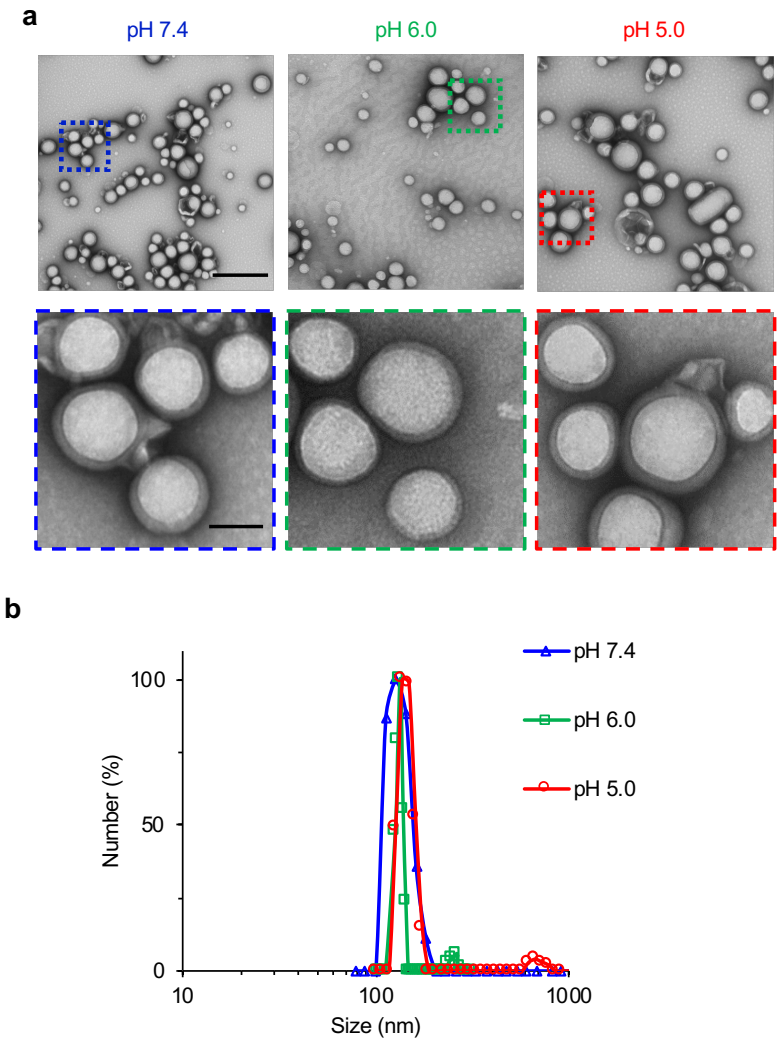

Supplementary Fig. 4. Nanoparticles synthesized using chitosan-guanidinate without CO_2 are not pH responsive. a, TEM images of the nanoparticles under different pH conditions showing that nanoparticles could maintain their intact spherical morphology and core-shell structure and are not responsive to low pH treatment (pH 6.0 and pH 5.0). **b,** Nanoparticle size distribution determined by dynamic light scattering (DLS) at pH 7.4, 6.0, and 5.0, respectively. Scale bars: 500 nm for top row and 100 nm for bottom row. The experiments were repeated three times independently.

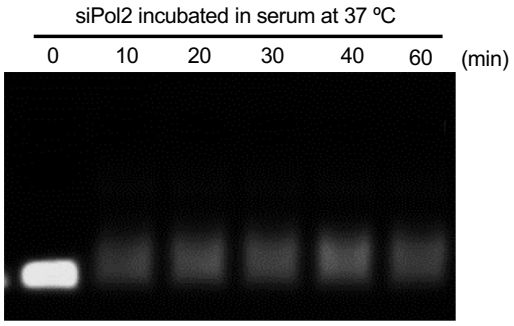

Supplementary Fig. 5. **Electrophoretic stability assay of free siPOLR2A.** The siRNA was incubated in serum at 37 °C for up to 60 min. The data indicate most of the free siRNA degraded in serum in less than 10 minutes. The experiments were repeated three times independently.

a

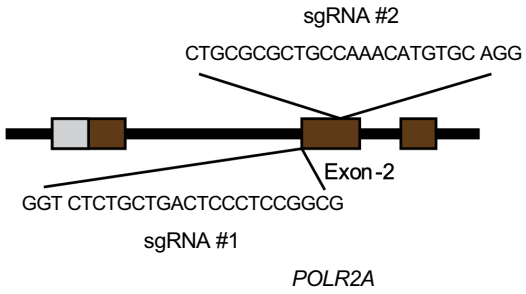

b

Loss-1

```
cDNA    115 GGTGGCATCAAATACCCAGAGACGACTGAGGGAGGCCGCCCCAAGCTTGGG  166
Protein  38 -G--G--I--K--Y--P--E--T--T--E--G--G--R--P--K--L--G-   54
Loss #1 115 GGTGGCATCAAATACCCAGAGACGA--------GGCCGCCCCAAGCTTGGG  166
```

Loss-2

```
cDNA    190 TGATTGAGCGGACTGGCCGCTGCCAAACATGTGCAGGAAACATGACAGAGTGTC  244
Protein  64 V--I--E--R--T--G--R--C--Q--T--C--A--G--N--M--T--E--C--   80
Loss #2 190 TGATTGAGCGGACTGGCCGCTGCCAAACAT----AGGAAACATGACAGAGTGTC  244
```

c

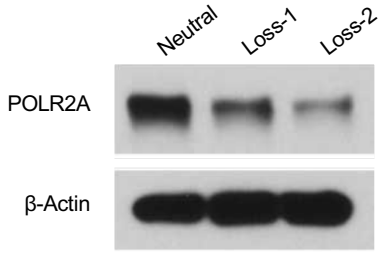

Supplementary Fig. 6. Generating isogenic HCC1937 cell lines bearing hemizygous loss of *POLR2A*. a, A schematic illustration of the Cas9/sgRNA-targeting sites in the *POLR2A* gene. **b**, Sequences of mutant POLR2A alleles in the isogenic colonies. Protospacer adjacent motif (PAM) sequences are highlighted in red. Small deletions in the targeted region lead to an open reading frame shift, producing only a short stretch of the amino-terminal peptide without any functional domains of POLR2A. **c**, Protein levels of POLR2A in *POLR2A*^{neutral} and *POLR2A*^{loss} HCC1937 cells. The experiments were repeated three times independently.

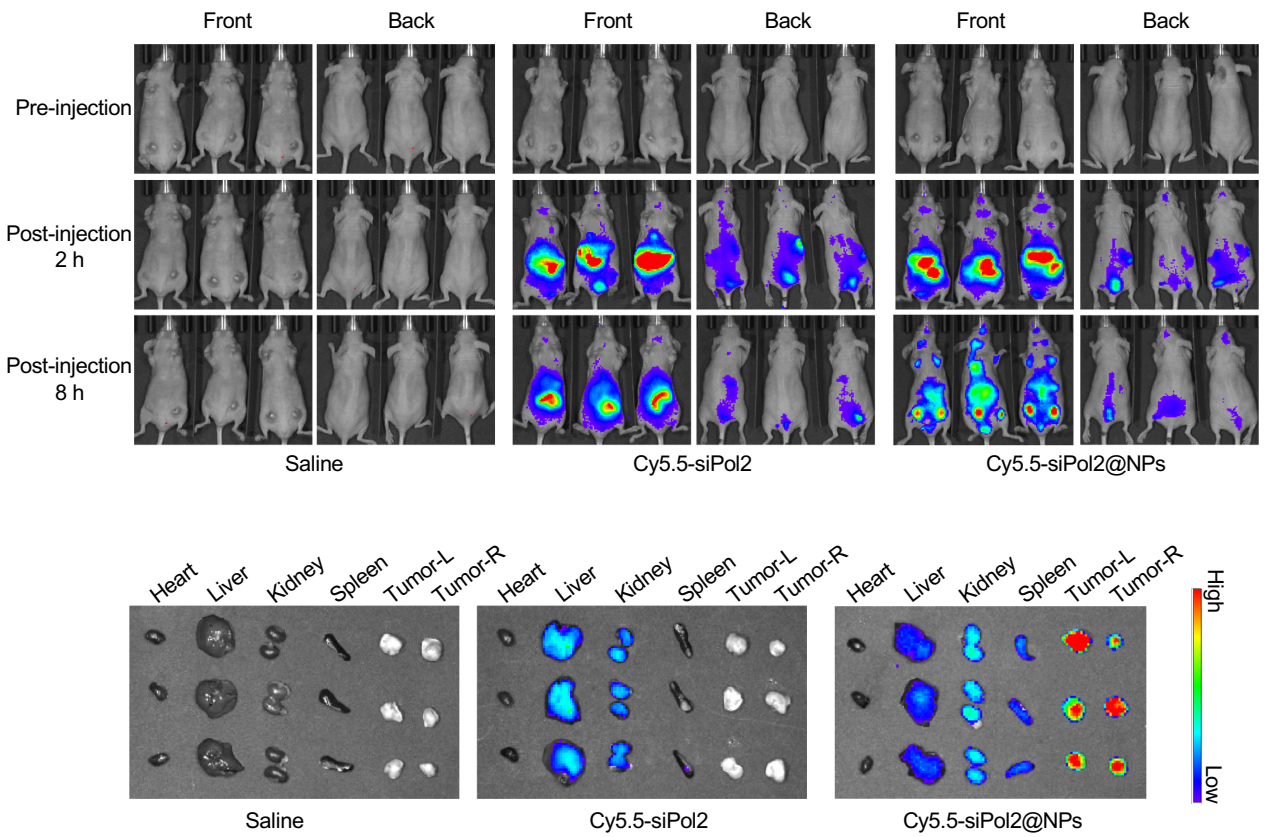

Supplementary Fig. 7. Whole body and organ biodistribution of nanoparticles. Top: in vivo whole animal imaging (both front and back) of Cy5.5 fluorescence at pre-injection, and 2 and 8 h after intravenous injection of saline, free Cy5.5-siPol2, and Cy5.5-siPol2@NPs. Three mice were used for each of the three experimental conditions. Bottom: ex vivo imaging of Cy5.5 fluorescence in tumours together with four critical organs collected after in vivo imaging at 8 h. Tumour-L and Tumour-R denote tumour on the left and right of the mouse, respectively (n=3 biologically independent samples).

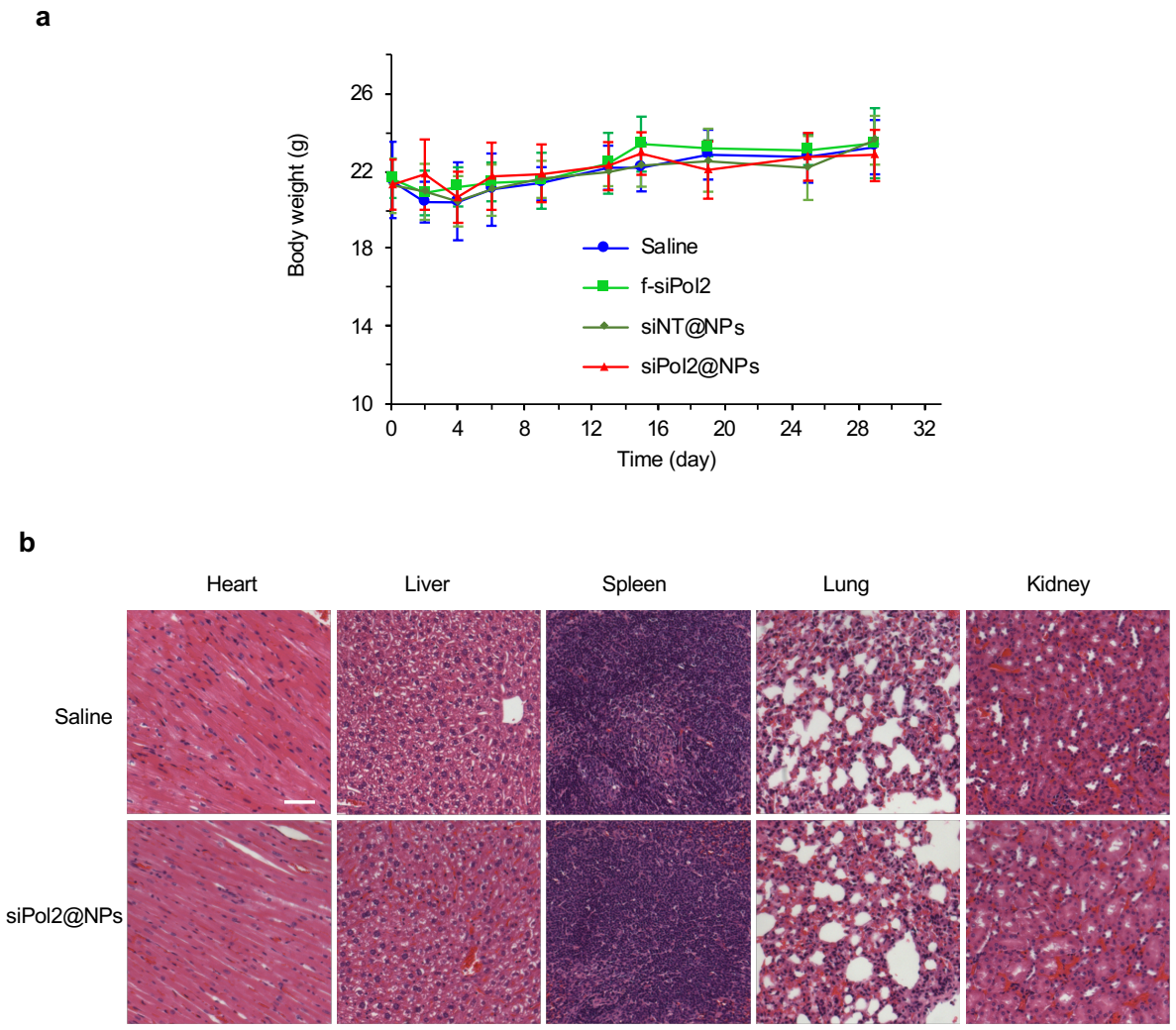

Supplementary Fig. 8. No evident systemic toxicity for the nanoparticle mediated delivery of siPol2 to isogenic tumours. a, Body weight of mice with various treatments showing no significant difference between the different treatments. Tumours were established by implanting isogenic HCC1937 (*POLR2A*^{loss}) cells on the left and parent HCC1937 (*POLR2A*^{neutral}) cells on the right. Error bars represent s.d. (n=7 biologically independent samples). **b,** Representative H&E-stained slices of major organs in mice treated with siPol2@NPs or saline collected on day 30. The experiments were repeated three times independently. Scale bar: 100 μm.

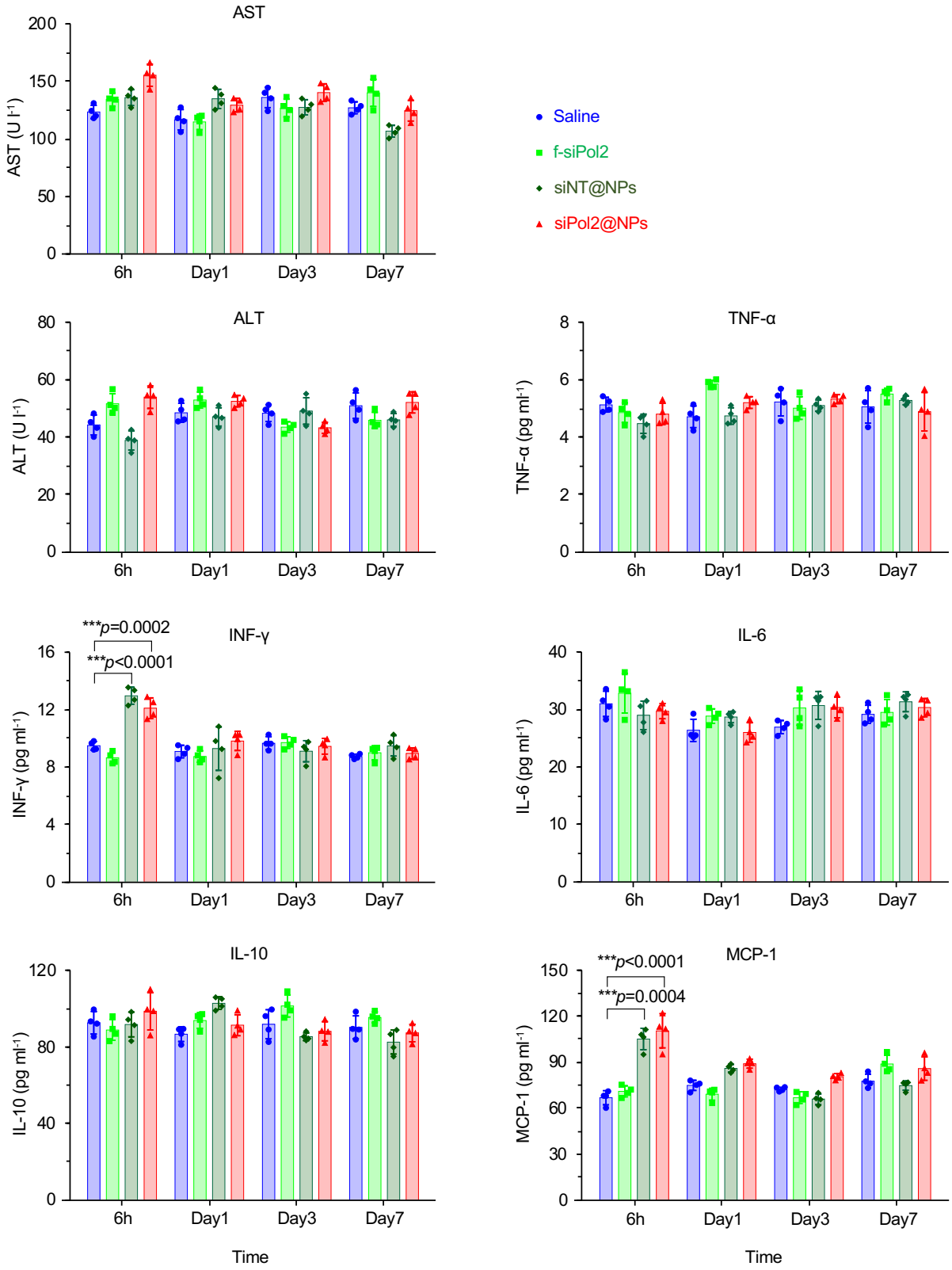

Supplementary Fig. 9. Negligible liver toxicity and immune response induction by nanoparticles. No significant different difference was observed for the two liver enzymes: aspartate aminotransferase

(AST) and alanine aminotransferase (ALT). Significantly increased levels of IFN-γ and MCP-1 were observed only for the siNT@NP and siPol2@NP treatments at 6 h after injection, which returned to the baseline levels on day 1 and thereafter. TNF-α: tumour necrosis factor-α, IFN-γ: interferon-γ, IL-6: interleukin-6, IL-10: interleukin-10, and MCP-1: monocyte chemoattractant protein-1. The biologically independent sample size n=4. Error bars denote mean ± s.d., ***: $p < 0.0001$. The statistical significance was assessed by one-way ANOVA with a Dunnett's post-hoc test.

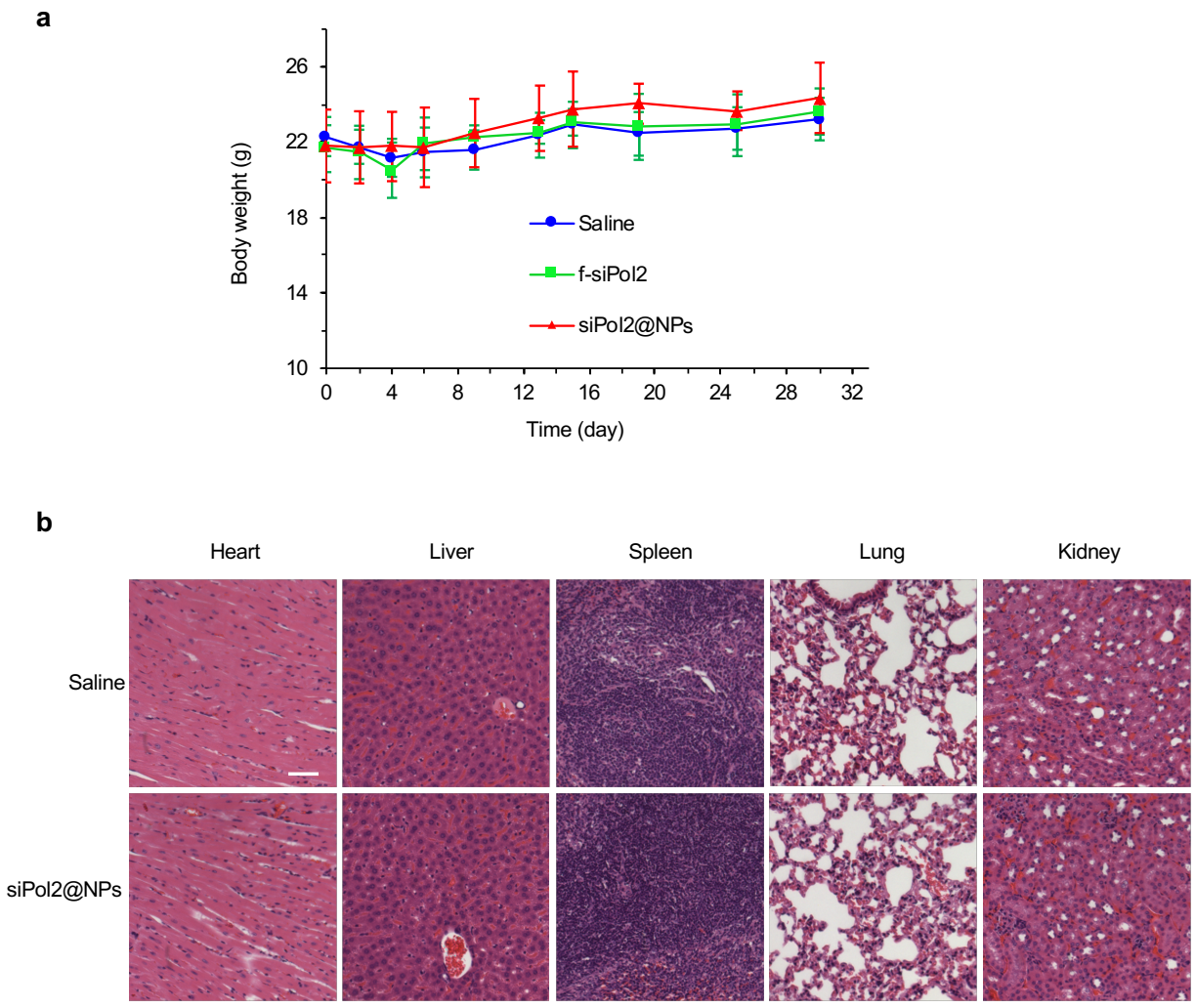

Supplementary Fig. 10. No evident systemic toxicity for the nanoparticle mediated delivery of siPol2 to wild type cells derived tumours. a, Body weight of mice with various treatments showing no significant difference between the different treatments. Tumours were established by implanting MDA-MB-453 (*POLR2A*^{loss}) cells on the left and MDA-MB-231 (*POLR2A*^{neutral}) cells on the right. Error bars represent s.d. (n=6 biologically independent samples). **b,** Representative hematoxylin & eosin (H&E)-stained slices of major organs in mice treated with siPol2@NPs or saline collected on day 30. The experiments were repeated three times independently. Scale bar: 100 μm.

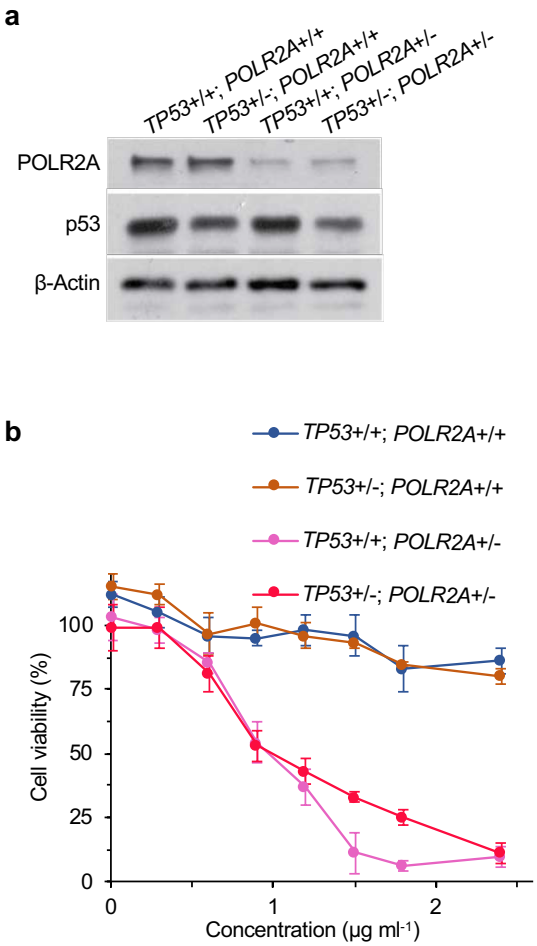

Supplementary Fig. 11. *POLR2A*^{loss} cells highly sensitive to POLR2A inhibition regardless of their *TP53* status. a, Protein level of POLR2A and p53 of four different isogenic HER18 HER2+ breast cancer cell lines. The experiments were repeated three times independently. **b,** Two *POLR2A*^{loss} HER18 (*TP53*$^{+/+}$, *POLR2A*$^{+/-}$ and *TP53*$^{+/-}$, *POLR2A*$^{+/-}$) cell lines and two *POLR2A*^{neutral} HER18 (*TP53*$^{+/+}$, *POLR2A*$^{+/+}$ and *TP53*$^{+/-}$, *POLR2A*$^{+/+}$) cell lines are treated with different dosages siPol2 in the form of siPol2@NPs for 72 h. Quantitative analyses of the cell viability using crystal violet staining are shown (n = 3 independent experiments with 3 replicates in each experiment). Error bars denote mean ± s.e.m.

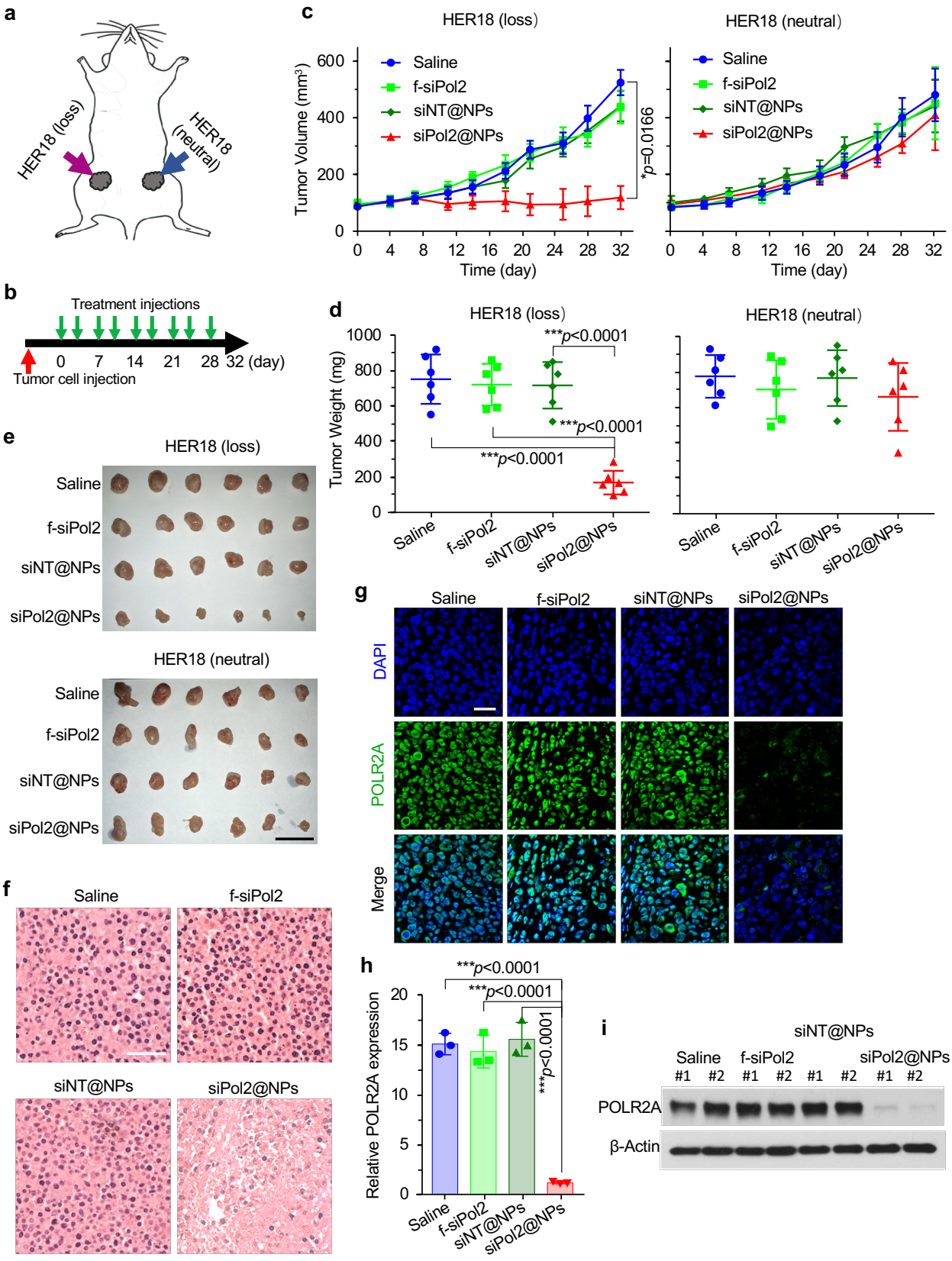

Supplementary Fig. 12. Targeted POLR2A inhibition for treating HER2+ breast cancer. a, A

schematic illustration of the tumours established by implanting isogenic HER18 (*TP53*$^{+/+}$, *POLR2A*$^{-/+}$, or *POLR2A*^{loss}) cells on the left and parent HER18 (*TP53*$^{+/+}$, *POLR2A*$^{-/+}$, or *POLR2A*^{neutral}) cells on the right 4th inguinal mammary fat pads. **b,** An illustration of the treatment intervals. The mice were injected with the various treatments twice a week. **c-e,** Tumour growth (**c**), weight (**d**), and gross images (**e**) of tumours derived from isogenic *POLR2A*^{loss} and parent *POLR2A*^{neutral} HER18 cancer cells with various treatments. The data indicate that tumours with hemizygous loss of *POLR2A* are highly sensitive and vulnerable to further POLR2A inhibition. Error bars denote mean ± s.d. In c, he p values for comparisons of siPol2@NPs versus Saline, siPol2@NPs versus f-siPol2, and siPol2@NPs versus f-siPol2 are 0.0166 (indicated in c), 0.0063, and 0.0142, respectively. The statistical significance was assessed by one-way ANOVA with a Fisher's LSD post hoc test for c or Dunnett's post hoc test for d. The biologically independent sample size n=6. Scale bar: 2 cm. **f-g**, H&E staining (**g**) and immunofluorescence staining (**g**) of *POLR2A*^{loss} tumours from the four different treatments. The experiments in f were repeated three times independently. **h-i,** Quantitative (**h**) and qualitative (**i**) data of POLR2A expression in the aforementioned *POLR2A*^{loss} tumours with various treatments (n=6 biologically independent samples). In h, the statistical significance was assessed by one-way ANOVA with a Dunnett's post hoc test. In i, two representative samples for each treatment are shown. Error bars denote mean ± s.d., *: $p < 0.05$; and ***: $p < 0.001$. Scale bar: 50 μm.

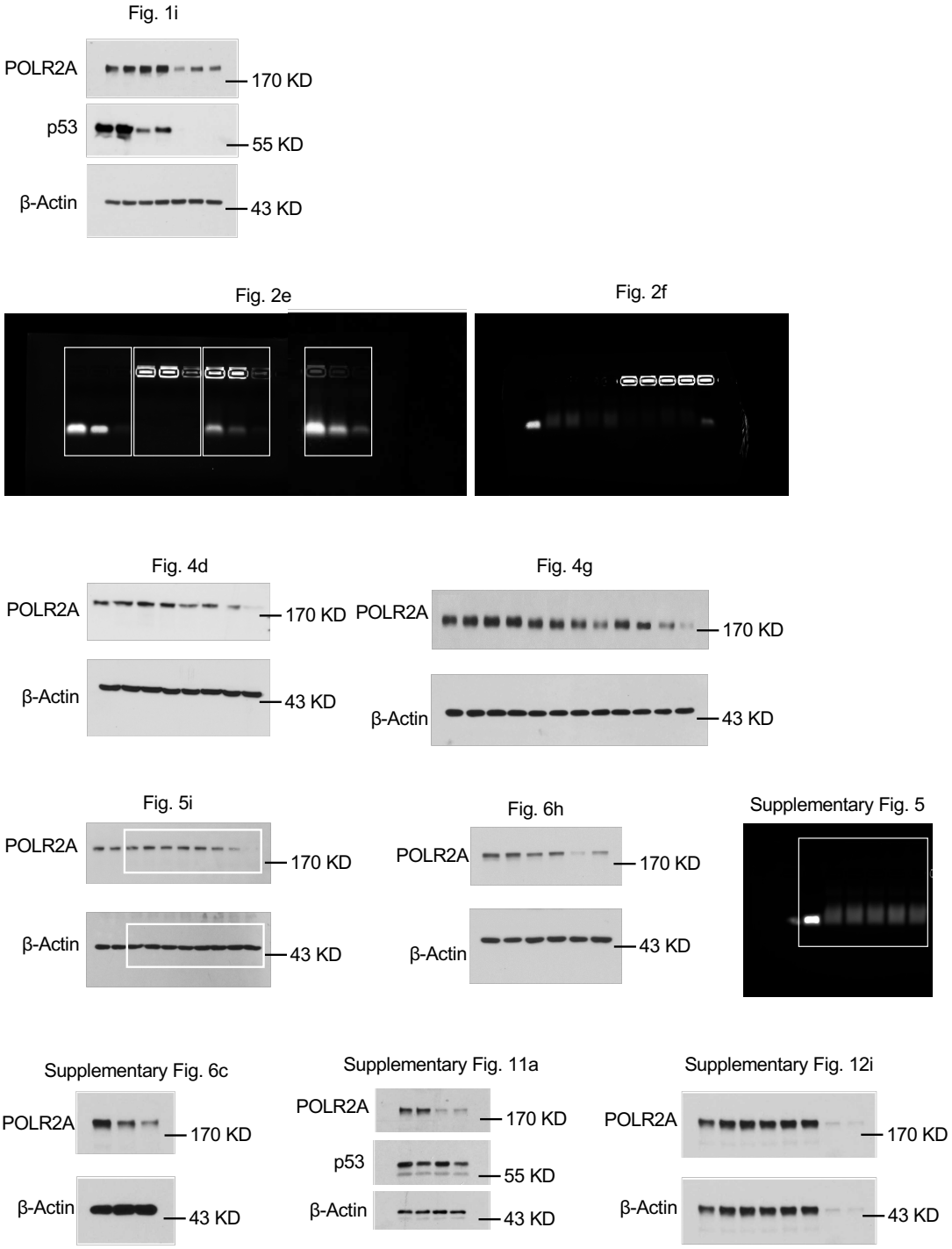

Supplementary Fig. 13. Uncropped western blots and gels. White rectangles indicate lanes used in the specific figures given above the blots and gels.

Supplementary Notes

Supplementary Note 1: As shown in **Fig. 1c**, hemizygous loss of *TP53* occurs in approximately 75% of HER2 positive (HER2+) breast cancer. Even though there are a variety of approved therapies for treating HER2+ breast cancer, acquired resistance to its therapy remains universal and approaches are still in need to address it. Therefore, we further investigated the potential applications of using siPol2@NPs to precisely target *POLR2A* in HER2+ subtype breast cancer. To further confirm our hypothesis that POLR2A targeted therapy is independent of the p53 status, we generated three isogenic HER18 cell lines of HER2+ breast cancer ($TP53^{+/-}$, $POLR2A^{+/+}$; $TP53^{+/+}$, $POLR2A^{+/-}$; $TP53^{+/-}$, $POLR2A^{+/-}$) using the CRISPR/Cas9 technology (**Supplementary Fig. 11a**) from the parent HER18 cells ($TP53^{+/+}$, $POLR2A^{+/+}$). As shown in **Supplementary Fig. 11b**, the two HER18 cell lines with $POLR2A^{loss}$ ($TP53^{+/+}$, $POLR2A^{+/-}$ and $TP53^{+/-}$, $POLR2A^{+/-}$) are significantly more sensitive to the *POLR2A* knockdown in comparison with the other two HER18 cell lines with $POLR2A^{neutral}$ ($TP53^{+/+}$, $POLR2A^{+/+}$ and $TP53^{+/-}$, $POLR2A^{+/+}$). To test our strategy for treating HER2+ human breast cancer in vivo, we established HER2+ breast tumours in nude mice using the isogenic HER18 cells ($TP53^{+/+}$, $POLR2A^{+/-}$) and the parent HER18 cells ($TP53^{+/+}$, $POLR2A^{+/+}$) as illustrated in **supplementary Fig. 12a-b.** Inhibiting POLR2A by siPol2@NPs significantly reduced the $POLR2A^{loss}$ tumour growth by ~75% (**Supplementary Fig. 12c-e**) in all six mice compared to the tumour from the control (saline) group. POLR2A protein levels in the siPol2@NPs treatment group were minimized (**supplementary Fig. 12f-i**). This observation in the HER2+ tumour model is consistent with that observed in the TNBC mouse models. These results confirm that further *POLR2A* silencing in cancer cells containing hemizygous *TP53* deletion leads to tumour suppression, and the POLR2A targeted therapy with siPol2@NPs is a promising therapeutic approach for both TNBC and HER2+ breast cancer and possibly other breast cancer subtypes.

Supplementary Note 2: The hemizygous deletion of *TP53*, which often involves a large fragment (over several megabases), even the whole short arm of chromosome 17 (17p), is a frequent genomic event across many types of human cancers. In tumours with hemizygous loss of *TP53*, *POLR2A* is almost always co-deleted. As an example, 99.5% (575 out of 578) of human breast cancers with hemizygous loss of *TP53* contain co-deletion of *POLR2A*. In clinical practice, the copy number of *TP53* gene has been examined by fluorescence in situ hybridization (FISH). The use of archival frozen tumour tissue imprint specimens for FISH has been well established in the clinic. Quantitative PCR and SNP DNA microarrays are also feasible to detect copy number changes of *TP53* and *POLR2A*. Based on the extensive cancer genomics data, it appears to be unnecessary to check the heterozygous deletion of *POLR2A* in the cancers harbouring hemizygous loss of *TP53*. Approximately half of human breast cancers with hemizygous loss of *TP53* harbours mutant *TP53* on the remaining allele, in support of the two-hit hypothesis in human cancer. However, the sensitivity of cancer cells to POLR2A inhibition appears to be primarily dependent on the status of *POLR2A*, regardless of *TP53* status. Moreover, given the prevalence of *TP53* loss in all breast cancer subtypes as well as other types of human cancer, the principle of essential lethality to POLR2A inhibition can also be applied to other human cancers including HER2+ breast cancer. Over the last few years, the rapid development of high throughput platforms such as microarrays and next generation sequencing technologies offers a promising prospect for the translation of our POLR2A-targeted therapy.

Our knowledge and arsenal of cancer nanomedicine have rapidly expanded in the past several years[1]. However, only few nanoparticle-based RNAi therapeutics have entered the clinical trial phase[1-4]. Lipid nanoparticles or liposomes-based delivery of siRNA is the most investigated approach in clinical trials[5]. Unfortunately, this approach has not reached Phase II/III stages of clinical trial. One of the major reasons is that it cannot achieve endo/lysosomal escape to allow the siRNA to reach the RNA-Induced Silencing Complex (RISC) located in the cytoplasm. Endo/lysosomal escape of siRNA is essential because the RNases inside the endo/lysosomes could quickly degrade the therapeutic agent before it

can reach its target. Unlike the liposomes-based approach, our pH-activated “nano-bomb” nanoparticles were designed for enhanced cytosolic delivery of siRNA because it can respond to the low-pH environment in endo/lysosomes to quickly release most of the encapsulated siRNA before it is degraded. This leads to a highly efficient utilization of the siRNA, which promotes high therapeutic efficacy with minimized siRNA dose compared to the liposomes-based approach. Moreover, tumour cells harbouring hemizygous deletion of *TP53*, which is a common genetic alteration in cancer, are markedly sensitive to further POLR2A inhibition. In other words, low dosage of siPol2@NPs could be used to kill *POLR2A*^{loss} cells (tumour cells) but not *POLR2A*^{neutral} cells (healthy cells). Another major reason causing nanomedicine to fail in clinical trial (phase I) is the undesired side effect[3,5]. Our nanoparticles are synthesized using FDA-approved biocompatible materials, which should minimize the undesired side effect. Therefore, our siPol2@NPs capable of quickly escaping endo/lysosomes triggered by low pH and precisely targeting *POLR2A*^{loss} cancer cells have tremendous potential for effective and safe delivery of siRNA to treat patients with cancer harbouring hemizygous loss of *POLR2A* regardless of the *TP53* status.

References

1. Shi, J., Kantoff, P. W., Wooster, R., Farokhzad, O. C. Cancer nanomedicine: progress, challenges and opportunities. *Nat. Rev. Cancer* **17,** 20 (2016).
2. Wittrup, A., Lieberman, J. Knocking down disease: a progress report on siRNA therapeutics. *Nat. Rev. Genet.* **16,** 543 (2015).
3. Bobbin, M. L., Rossi, J. J. RNA Interference (RNAi)-Based Therapeutics: Delivering on the Promise? *Annu. Rev. Pharmacol. Toxicol.* **56**(1)**,** 103-122 (2016).
4. Dahlman, J. E.*,* et al. In vivo endothelial siRNA delivery using polymeric nanoparticles with low molecular weight. *Nat. Nanotechnol.* **9,** 648 (2014).
5. Blanco, E., Shen, H., Ferrari, M. Principles of nanoparticle design for overcoming biological barriers to drug delivery. *Nat. Biotechnol.* **33,** 941 (2015).